

Printable properties of cementitious material containing copper tailings for extrusion based 3D printing

Guowei Ma ^{a,b}, Zhijian Li ^c, Li Wang ^{a,*}

^a School of Civil and Transportation Engineering, Hebei University of Technology, 5340 Xiping Road, Beichen District, Tianjin 300401, China

^b School of Civil, Environmental and Mining Engineering, The University of Western Australia, Crawley, WA 6009, Australia

^c College of Architecture and Civil Engineering, Beijing University of Technology, 100 Pingleyuan, Chaoyang District, Beijing 100124, China

HIGHLIGHTS

- Printable properties of mixtures with six substitute ratios of tailing to sand are investigated.
- Optimal mixture that enables structures achieve a favourable buildability is determined.
- Critical value of controlling parameters to achieve sufficient printability are specified.
- Mechanical strength of the printed and the casted samples are measured.
- Extrudability and buildability coefficients are firstly proposed for optimizing design.

ARTICLE INFO

Article history:

Received 11 May 2017

Received in revised form 7 November 2017

Accepted 6 December 2017

Keywords:

3D printing

Cementitious material

Printability

Fresh property

Extrudability

Buildability

ABSTRACT

3D printing for cementitious material is an innovative and promising construction method that is rapidly gaining ground in recent years. Utilizing waste or recyclable materials as the primary raw material to produce cementitious material for 3D printing can greatly promote the 3D printing to reach its maximum cost-effective potentials. This paper proposes an environmental friendly cementitious mixture that is compatible with an extrusion based printing process. In this study, six replacement ratio of tailing to sand from 0% to 50% are investigated. A single nozzle printing system is developed and the operational process is illustrated. Experimental tests are performed to determine the printable properties of mixtures containing various content of tailings, including the extrudability, buildability, flowability, open time, fresh and hardened properties, etc. Based on the measurements, the optimal mixture is determined as substituting natural sand with 30% mass ratio of mining tailings, which enables structures achieve a favorable buildability and a relatively high mechanical strength. In particular, the critical value of controlling parameters to achieve sufficient printability are specified. And the compressive and flexural strength of the printed and the casted samples are measured and compared. To conclude the present research, extrudability and buildability coefficients are proposed for optimizing design.

© 2017 Elsevier Ltd. All rights reserved.

1. Introduction

3D printing is a novel and promising process to build up structures in a layer by layer manner based upon a computer designed file, which has been successfully applied in various fields [1–4]. Recently, the building industry has made a series of attempts to apply this technique on a practical construction scale due to its outstanding flexibility in both architectural and structural design. Premixed materials are extruded through a nozzle to build structural components layer-upon-layer without the facilitation of

formwork or any subsequent vibration [5–8]. Various manufacturing methods of largescale 3D printing have been continuously developed and improved. Contour crafting developed by Dr. Behrokh Khoshnevis is a well-known process for construction-scale 3D printing [9]. Some specific implementation practices have been presented. For example, the five-story apartment 3D printed by WinSun [10], the BigDelta project [11] of a castle printed in-situ [12], etc., which have all demonstrated the great potential and feasibility of 3D printing in constructing large-scale building components.

Rapid application of this innovative technique in the construction field rely on the development of high performance cementitious materials that are compatible with 3D printers. Le et al.

* Corresponding author.

E-mail address: wang1@126.com (L. Wang).

[13] developed a high-performance fiber reinforced printing mixture for concrete printing process. A high cementitious materials content of low water/cementitious materials ratio of 0.26 was employed to achieve desirable fresh state properties and a 28-day compressive strength of 110 MPa. Pshtiwan et al. [14] proposed a new type of 3D printing powder modified by cement powders which is designed to fabricate scaffold (structure) by powder based 3D printer. Manuel et al. [15] provided first insights into a 3D-printed composite of Portland cement paste and reinforcing short fibers (carbon, glass and basalt fibers), which exhibit high flexural (up to 30 MPa) and compressive strength (up to 80 MPa). Gosselin et al. [16] developed an ultra-high performance concrete for large-scale 3D printing system. Even though, it is still of high requirement to expand the current severely limited scope of materials that can be used in an extrusion based 3D printing process.

Mine tailings (MT) are the solid residues left after valuable minerals have been extracted from the ores. Few reuse and large stockpile of tailings have led to a number of environmental, financial and social problems [17,18]. Disposal of mine tailings have been a major concern in mining industry [19,20]. Utilizing mining tailing as the primary raw material to produce cementitious material for 3D printing can greatly promote the 3D printing to reach its maximum cost-effective and environmental-friendly potentials. From another aspect, it is also in agreement with the objective of strategy of resources recycling and building energy efficiency of China. In current practice, mine tailings have been utilized as a kind of substitute material for concrete mixtures and the feasibility of utilizing mine tailings for production of eco-friendly materials has been validated [21–25]. However, despite some explorations have been conducted regarding to adopting the mining tailings in concrete preparation, the application of tailings in cementitious materials for 3D printing is extremely insufficient and the coordination effect with printing systems is yet to be explored.

Appling mining tailings as the raw material for extrusion based 3D printing shall meet certain vital criteria to be compatible with

the printing processes. Different from the castable concrete, the mixtures are designed to be easy-extrusive, low-slump, well-buildable, fast-setting and with good mechanical strength in order to produce a continuous paste from the printing nozzle and to ensure a rapid modelling of freeform construction [7,26–28]. The goal of the printability controlling is to ensure that each printed layer has the capacity to retain its original shape and sustain subsequent layers right after extrusion, and yet stay viscous enough to bond the adjacent layers avoiding the formation of a separate voids. There exists a sensitive balance between the material properties (flowability, extrudability, buildability, open time, etc.) and the process parameters (printing speed, nozzle opening, extrusion rate, etc.) [29,30]. Ali Kazemian et al. [31] proposed a series of test methods for evaluation of the printing quality and shape stability of fresh mixtures. In particular, the time limit for printability and blockage are suggested and specified.

Despite several cement-based materials for 3D printing in construction sector have been proposed, attempts and studies are little available about the application of mining tailings in manufacturing cementitious materials for 3D printing. A series of tests have been conducted to investigate the relevant extrudability, buildability, flowability, open time, fresh and hardened properties of the proposed material to find the optimal mixture proportion that is well compatible to the printing process. In particular, the critical values of controlling parameters to achieve sufficient printability are specified. And the compressive and flexural strength of the printed and casted samples are measured and compared. This research develops eco-friendly materials for 3D printing, improves the efficiency in resource management and the automation in construction industries.

2. Cementitious material extrusion system

Fig. 1 illustrates schematically the set-up of a cementitious material extrusion system. In general, this system comprises of a

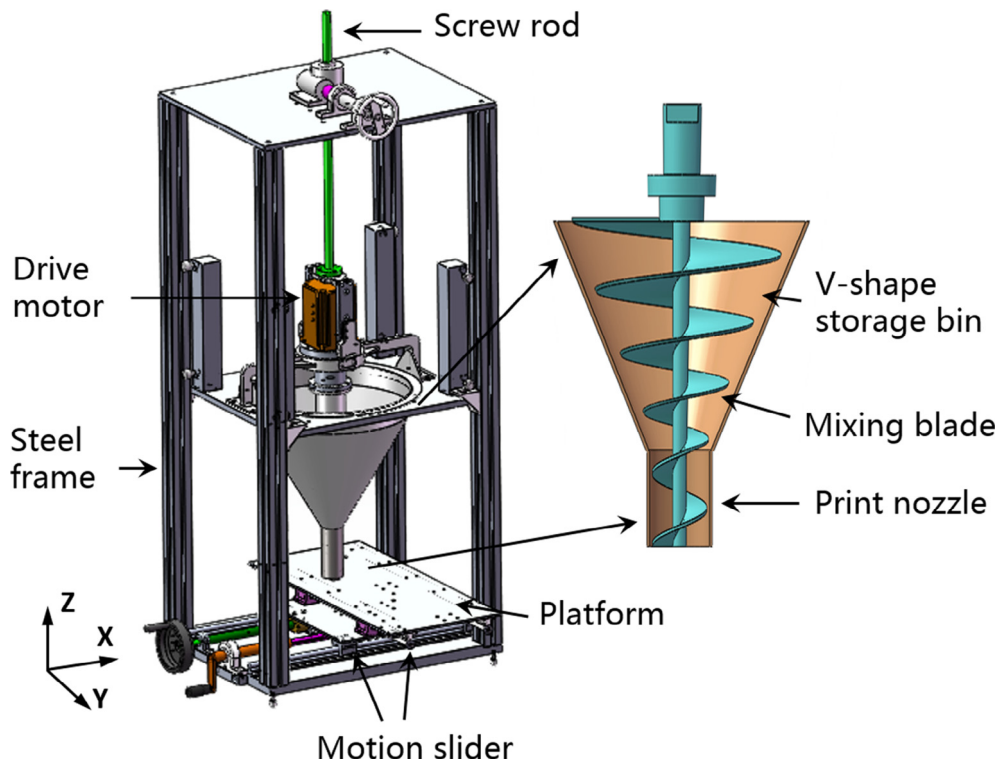


Fig. 1. Design sketch of the cementitious material extrusion system.

steel frame, a V-shape storage bin, motion sliders, platform, mixing blade and drive motors. The size of the steel frame is 0.5 m (L) \times 0.39 m (W) \times 1.1 m (H). The V-shape storage bin containing the freshly prepared cementitious materials is connected to the steel frame by means of a vertical screw rod and four motion wheels. Particularly, an awl-shaped mixing blade is equipped inside the storage bin. The rotation of the blade is controlled by a drive motor with adjustable speed to transport the cement paste to the nozzle. The drive motor is mounted on a screw rod which controls the motion of storage bin in the Z direction. At the bottom of the V shape tank it is the printing nozzle with an opening of 8 \times 30 mm. A platform (40 cm \times 20 cm) used to place the 3D printed models is located at the bottom of the steel frame. It can freely move in X and Y directions through a series of transmission components that connected to the steel frame.

This study is our preliminary attempt to investigate the extrusion process of proposed cementitious material and evaluate its coordinating effect with the printing system. We do not consider the pumping delivery system at the current stage. The cementitious material is manufactured through conventional mixer, transported to the V-shape storage bin, and then conveyed to the bottom printing head through the mixing blade. Then the extruded cementitious paste are laid down to the platform. The 3D design is completed in a layer by layer process through a combined motion of the platform in X and Y direction and the storage bin in the Z direction.

3. Materials and testing procedures

3.1. Material preparation

Rapid hardening Portland cement P. O 42.5R with a 3-day static compressive strength of 22.0 MPa, fly ash and silica fume are used as the binding materials. Local river sand with a specific surface area of 0.101 m²/g and copper tailings with a specific surface area of 0.141 m²/g serve as the fine aggregates. The tailings are obtained from a copper mine located in Dongchuan City, China. Besides, high efficient polycarboxylate-based superplasticizer with a water reducing rate of more than 30% and a solid content fraction of 37.2% are adopted to achieve the required flowability for the mixture. Additionally, a small amount of polypropylene (PP) fibers are employed to reduce the formation of shrinkage due to early drying. This is highly important for the printing concrete since the

relatively large area of free surfaces can enable a high rate of water evaporation. The specifications of PP fibers are listed in Table 1. The chemical compositions of the natural sand and tailing have been determined by the X-ray fluorescence (XRF) analysis. The results listed in Table 2 indicate that tailings are comprised of silica, calcium, alumina and iron oxide and free of hazardous industrial waste elements.

The mass ratio substitution of copper tailing to natural sand of samples that are denoted by R0, R10, R20, R30, R40, R50 are 0%, 10%, 20%, 30%, 40%, and 50%, respectively. Table 3 shows the mass ratios of the raw materials used for material preparation. PP fibers and the dry powders, i.e., cement, fly ash, silica fume, natural sand and tailings are firstly mixed and blended for three minutes to obtain a uniform mixture and to make the fine powders separate fibers into balls during the mixing process. Then, one half of the total amount of water along with the superplasticizer is added in and stirred for two minutes. Subsequently, the second half of the total amount of water together with superplasticizer is poured in and stirred for an additional two minutes. Afterwards, the mixture is delivered to the single nozzle printing system to evaluate their printable abilities.

3.2. Determination of particle size distribution

Cementitious materials for 3D printing need to have a smooth grading of materials to ensure a favorable degree of extrudability and flowability. Good grading of materials provide a stable compounding structure, thus maximizing the skeleton and stabilization performance of particles [32,33]. Meanwhile, a proper grading facilitates the particles to form a dense filling system, which ensures a higher water retentivity and contributes to the workability of mortars. It is therefore necessary to measure the particle size distribution of the cementitious materials. The particle size distribution of the river sand and tailings as well as the particle size distribution of various dry powder mixtures of sample R0 – R50 with different tailing contents are measured through a laser diffraction particle size analyzer.

3.3. Evaluation of printability

The choice of the optimal mix for 3D printing necessitates several tests to be conducted. The printing abilities of cementitious materials with different tailing replacement ratios are then

Table 1

Specifications for the polypropylene fibers.

Properties	Length (mm)	Diameter (μm)	Density (g/cm ³)	Elastic modulus (GPa)	Tensile strength (MPa)	Linear strain at failure
Quantity	9	23	0.91	3.0	3.5	80%

Table 2

Chemical Composition of tailings by mass ratio.

SiO ₂	Al ₂ O ₃	Fe ₂ O ₃	CaO	MgO	SO ₃	Na ₂ O	P ₂ O ₅	K ₂ O	MnO
39.77	4.61	20.16	22.29	7.17	3.05	1.32	0.26	0.44	0.23

Table 3

Mixture proportions of the raw materials used for 3D printable cementitious material by mass ratio.

Mix No.	Natural sand	Tailings	Replacement (%)	Cement	Fly ash	Silica fume	Water	Superplasticizer	PP fiber (kg/m ³)
R0	1.2	0	0	0.7	0.2	0.1	0.27	0.0029	1.2
R10	1.08	0.12	10	0.7	0.2	0.1	0.27	0.0029	1.2
R20	0.96	0.24	20	0.7	0.2	0.1	0.27	0.0029	1.2
R30	0.84	0.36	30	0.7	0.2	0.1	0.27	0.0029	1.2
R40	0.72	0.48	40	0.7	0.2	0.1	0.27	0.0029	1.2
R50	0.60	0.60	50	0.7	0.2	0.1	0.27	0.0029	1.2

measured and investigated, including the extrudability, flowability, buildability, open time and the mechanical properties. All these factors contribute in equal importance to the printing process [8,34]. Below is the description of the test procedure to ensure the specified target criteria are met.

3.3.1. Extrudability

Extrudability is a critical parameter that reflects if the materials could be protruded as a continuous filament through the nozzles. It is primarily affected by the quantities and distributions of the dry constituents in the mix [35]. Referring to the method proposed by Le et al. [13], the extrudability of fresh paste is evaluated by the continuity and stability of the extruded filament from printing nozzle with an opening of $8 \times 8 \text{ mm}^2$, which is one third smaller than current one of $8 \times 24 \text{ mm}^2$. Each filament is designed as total continuous length of 2000 mm long in eight return processes. Each subsection of the filament is 250 mm long. The test shape is designed to represent the typical pattern of building freeform construction components. Better extrudability is characterized by a longer distance over which the filament can be extruded out without separation, and a smaller opening from which the filament can be stably deposited with no liquid drainage and no blockage of the nozzle. If the rate of extrusion process is slow compared to the hydraulic conductivity of the material, liquid phase can flow through the granular skeleton, leading to a blockage of extrusion [36–39]. It is significant to control the extrusion rate by taking the hydraulic conductivity of materials into account in order to reach a consistent printing.

3.3.2. Buildability

The critical step of creating 3D structures through 3D printing is the vertical stacking of layers of filament. Buildability is another critical parameter to evaluate the printable performance of concrete materials, which refers to the ability of material to retain its extruded shape and the resistance of the deposited wet material to deformation under load [13,27,40]. Mixed paste is stored in the reservoir and extruded from the nozzle to form layered structures. The structures are designed to vertically stack twenty layers of extruded filaments of length of 250 mm and width of 30 mm without collapse at a rest time of 10 min. The 10 min is designed to facilitate the evaluation of shape-retentivity and load-sustainability of various tailing materials and to avoid the formation of cold joints and weaken interfaces. The height of each layer is designed to be 8 mm and so the machine is designed to move up in 8 mm intervals. All 20-layer structures of each material are realized with the same process, intending to elucidate the influence of various tailing replacement on the layer stacking process and structural stability of printed structures. Then the average vertical strain ε_d of each printed layer is measured to characterize the shape retention of the fresh pastes. Meanwhile, a geometric factor P_{hw} calculated by the height to width ratio of the printed structures is proposed to describe the stability of the printed structures. The parameter ε_d is adopted to specify the buildability of cementitious materials.

3.3.3. Open time

Open time stands for the time interval within which the fresh materials maintain good workability for printing. It can be

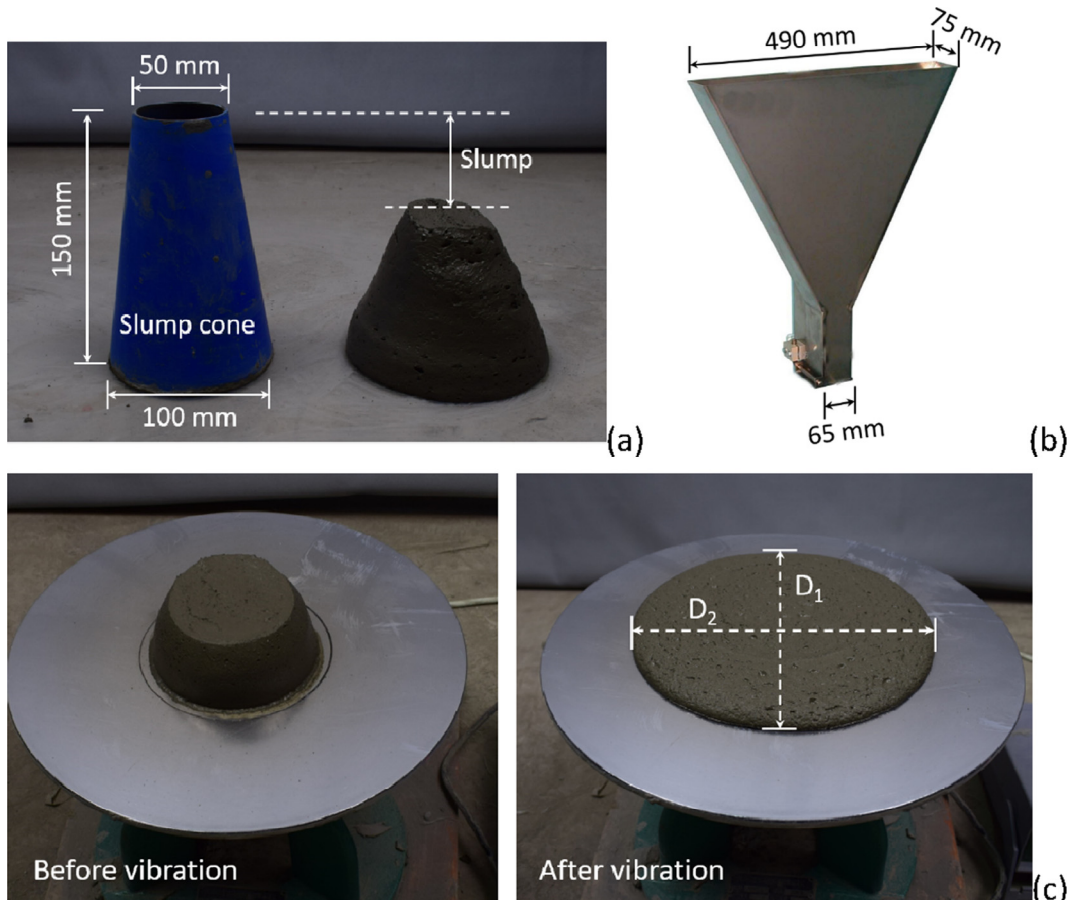


Fig. 2. (a) Slump test, (b) V-funnel test and (c) jump table test employed for flowability measurement.

measured with a Vicat apparatus or determined by the slump flow test to get the flowability over specific time intervals [41,42]. Le et al. [13] used the shear strength to determine the open time. The open time in our research is measured as the time period in which the fresh mixtures demonstrate acceptable extrudability. Simple structures are designed to be printed in two parallel lines (250 mm × 30 mm). The continuity of the filaments is investigated at rest time with intervals of 10 min. The open time t is ascertained once disruption of the filament occurs. Once this time period is determined, it can be used to recommend the range of slump and spreading diameter for acceptable flowability, and to specify the range of penetration resistance for acceptable structural build-up behaviors as the following sections discussed.

The extruded layer should have a short time to rest and build structure before the subsequent layer of concrete is deposited above it [43,44]. Therefore, the layers can maintain sufficient chemical activity to joint with the next layer in order to reach a successively printed structures. Otherwise, the finite “waiting time” between layers is prone to forming cold joints between layers. It may produce weak interfaces and result in certain mechan-

ical strength losses if a critical resting time is exceeded. The determination of open time should take both the cold joints problem and disruption of filaments into account.

3.3.4. Flowability

Flowability controlling is to ensure the smooth transportation of the fresh paste from the storage system to the nozzle. Measurement of flowability can be achieved by performing a series of experiments, including the slump test according to Chinese national testing standard GB/T 14,902–2012 [45], the V-funnel test according to JGJ/T283–2012 [46], and the jumping table test according to GB/T 2419–2005 [47].

The slump test is preferable in laboratories and on site mostly due to its simplicity and immediate results. As illustrated in Fig. 2, the slump cone has an internal diameter of 100 mm at the base and 50 mm at the top, and a height of 150 mm. The freshly mixed cement paste is placed into the cone. Then the flowability of materials is characterized by the drop in height of cement paste after the cone is removed. V-funnel test is then carried out to evaluate the viscosity of fresh concrete and the deformability to pass through the restricted areas [35]. In the current study, the V-shaped funnel shown in Fig. 2 is filled with fresh cement mortar. The elapsed time between opening the bottom outlet and complete emptying of the funnel is specified as the V-funnel flow time (V_t) [48]. In the jumping table test, a cone mould is filled with cementitious material and then the cone is removed. Subsequently, the table jumps for 25 times within the time of 25 ± 1 s, allowing the mixture to freely spread out. Thereafter, the average diameter of the spread concrete in two perpendicular directions is measured to indicate the flowability of the fresh cement paste. An easily expanding mix corresponds to a greater flowability.

3.3.5. Structural build-up behavior

Stiffness development is directly related to the buildability of printing materials since that the structures are printed in layers rather than entirely casted at once by formworks. The cementitious materials for 3D printing shall gain a relatively high mechanical stiffness at super-early ages to enable the build-up of structures to a large height [30]. In most cases, the printing materials are required to demonstrate enough stiffness within tens of minutes. However, due to the initial setting time of cement mortars are usually longer than ten hours, the parameters of initial setting time and final setting time are not applicable to evaluate the printing abilities of the materials.

As an alternative, the penetration resistance method is employed to access the stiffness development or structural build-up behavior of cementitious materials at the setting process. The experiments are conducted according to the Chinese national testing standard GB/T 50,080-2002[49]. The test uses a cone mould with an inside diameter of 150 mm at the bottom, an inside diameter of 160 mm at the top, and a height of 150 mm. The fresh cement mortar is firstly placed into the mould. Then a steel nail with an area of 100 mm^2 is pressed into the mortar for a depth of 25 ± 2 mm. The penetration resistance force produced by the mortar in the penetration process is measured by means of a spring connected to the nail [50,51]. The penetration resistance force divided by the area of nail is determined as the penetration resis-

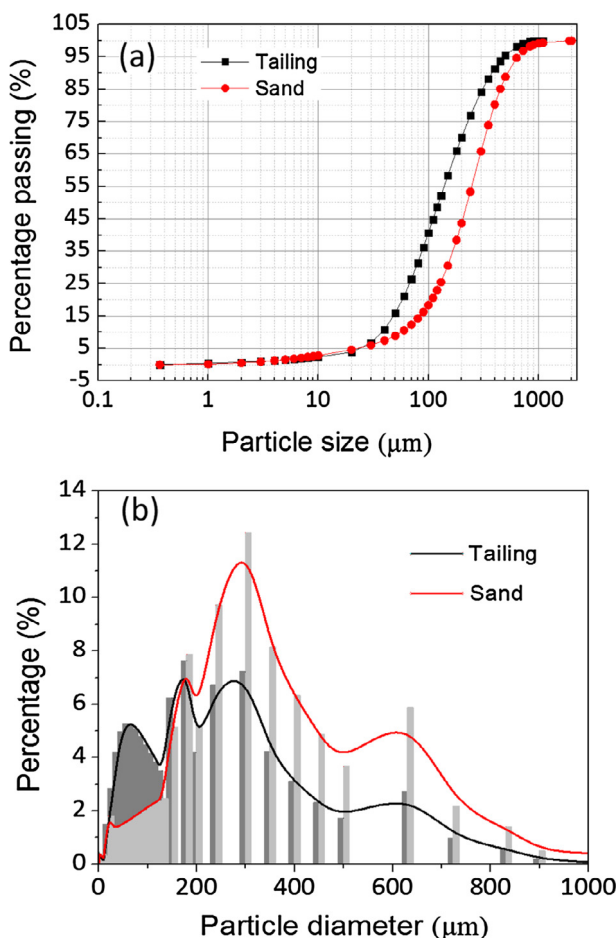


Fig. 3. (a) Particle size cumulative and (b) particle number percentage curve of natural sand and tailings obtained from laser diffraction.

Table 4

Particle size distribution parameters for natural sand and tailings.

	D[1,0] (μm)	d(0.1) (μm)	d(0.5) (μm)	d(0.9) (μm)	Average (μm)
Sand	375.61	56.52	225.57	519.92	378.5
Tailing	229.87	38.03	123.75	375.10	246.0

tance. At different rest times, the penetration resistance of various tailing materials are measured and recorded.

3.3.6. Hardened properties

The materials for 3D printing are also required to meet specific mechanical strength. Compressive strength of casted cubic samples fabricated with no rodding or consolidation are tested at the ages of 3, 14 and 28 days. The 7-day flexural strength of prism specimens cut from the 3D printed structures are measured through three points bending test. The flexural strength of casted prism specimens are also investigated as references. All the printed and casted samples are placed in the moist cabinet for proper curing with an ambient temperature of 20 ± 1 °C and the relative humidity of $95 \pm 5\%$ for seven days. Thereafter, the mechanical properties of hardened samples with varied tailing replacement ratios are then measured according to Chinese national testing standard GB/T 50,081-2002 [52]. Besides, a servo-control testing machine with loading capacity of 1500 kN is employed. The loading rate is set as 0.8 MPa/s and 0.05 mm/min for the compressive strength and three point bending test, respectively. Three cube specimens are tested repeatedly under the same loading conditions.

4. Result and discussion

4.1. Particle size distribution

The cumulative curve of particle volume percentages of sand and tailing are recorded and shown in Fig. 3(a). The results demonstrate that the natural sand and tailings show similar range of particle size from 1 to 1000 μm. However, the tailing curve is slightly shifted to the left, indicating that the tailings have smaller diameters than the sand. Then the results are recalculated as a particle number percentage as shown in Fig. 3(b). The number-based particle size distribution showed that the fraction of particles smaller than 50 μm and greater than 800 μm are negligible and that the majority of particles fall in the dimension of 100–500 μm. The average particle size of sand and tailing is 378.5 μm and 246.0 μm, respectively. The basic descriptive statistical particle size distribution parameters, i.e., the number weighted arithmetic mean D [1,0], d(0.1), d(0.5) and d(0.9), are presented in Table 4.

The d(0.1), d(0.5) and d(0.9) denote the size of the 10%, 50% and 90% of the particles measured are smaller than or equal to the size stated. The analysis results demonstrate that the tailings are finer than the natural sand. Therefore, replacing sands with tailings in the preparation process will influence the grading of the dry powders of materials. Table 5 lists the particle content of cementitious material with different tailing replacement ratios at three diameter intervals. It can be seen that the more tailings used, the higher percentage of dry powders range in the small diameter interval (0–130 μm).

4.2. Extrudability evaluation

A square opening (8×8 mm²) is contrived to observe the extrusion process of fresh pastes. A small opening provides a restrict requirement for a good extrudability. Fig. 4 presents the printed filament extruded from the square opening with a total length of 2000 mm. From our test results, all types of fresh mixtures performed good water retention properties and were continuously extruded without disruption, segregation and blockage, indicating acceptable extrudability. The test results also indicated that the extrusion rate is possible higher than the hydraulic conductivity of the material in the printing process. The applied extrusion rate and nozzle opening are in acceptable ranges for a successful 3D

Table 5

Particle content of dry mixtures at three diameter intervals.

Particle size interval (μm)	<130	130–250	250–500
R0	48.6	26.8	24.4
R10	50.4	26.7	22.7
R20	52.1	26.5	21.1
R30	53.9	26.3	19.4
R40	55.6	26.2	17.7
R50	57.4	26.0	16.1



Fig. 4. Filament of length of 2000 mm extruded from the small square nozzle.

printing. On the other hand, the filaments are relatively slender, which make them difficult to stack and sometimes twisting of the filament will take place. It is understood that the opening of the nozzle is a key parameter that directly related to the geometry of the extruded filament. An opening O_z in size of 8×24 mm² is designed to improve after several nozzle openings have been tried. The nozzles of 3D printer invented by Rudenko and Eindhoven University of Technology (TU/e) are square shaped with sizes of 30×10 mm and 40×10 mm, respectively [53,54]. The printing nozzles of concrete printer designed by Loughborough University is circular of \varnothing 6–20 mm, resulting in a layer thickness of 6–25 mm [27]. Hwang and Khoshnevis [55] report a similar circular nozzle of \varnothing 15 mm, which results in a layer thickness of 13 mm. Designing a smaller nozzle opening can realize more detailed features of the printed structures, which in turn sacrifice the construction efficiency.

Based on our experimental investigations, it is feasible for different printing process to produce a same result when the materials are different. However, when the material is fixed, there exists an corresponding printing process for it to reach an optimal printing results. There is a balancing and interrelated relationship of the extrudability of mixtures with the extrusion rate V_e and printing speed V_p . V_e is characterized by the extrusion rate of fresh paste, which is governed by the rotate speed of mixing blade. V_p refers to the moving speed of the nozzle. A set of trial and error tests have been carried out based on the nozzle of 8×25 mm². The extrusion rate is determined as 5.4 Ls/minute and the printing speed is controlled as 450 mm/min. Additionally, the height of the print head above the print surface H_p is also a critical factor that related to the printing process, which is illustrated in Fig. 5. In our tests, the H_p is set as equal to the nozzle opening width, i.e., 24 mm. Thereafter, O_z , V_p , V_e , and H_p associated with printing process are determined, which provide a fundamental base for the successful accomplishment of printing process.

4.3. Buildability evaluation

3D structures from 3D printing is to vertical stack layers of filament. The liquid and viscous property of fresh pastes are crucial to the bonding performance between layers, which greatly depends on the rest time. The shorter the rest time, the higher

bonding strength between layers. The bond strength between layers gradually improves when the printer speeds up. However, once the printer reaches a certain speed, the required strength of layers may not yet have enough time to develop. Thus, the load carrying capacity decreases with higher speeds.

In our test, all the structures are printed with a fixed printing speed of 450 cm/min and the time interval between adjacent layers is controlled as 30 ss. At the rest time of 10 mins, various mixtures containing different tailing content are extruded layer by layer at a vertical velocity of 1.3 cm/min until 20 layers of filaments were printed. Fig. 6 shows the final structures built-up with

twenty layers of filament in a single process by the proposed printing system. It could be observed that mixtures R0 – R30 performed good buildability. Namely, there is slightly change of the thickness of each layer, and all the layers are well vertically stacked and stand steadily without obvious deformation, sloping and collapsing. Although the studied materials may be still at the initial yield stress state, the prepared mixtures (R0-R30) are of great potential to perform favorable buildability when prolong the time to rest or the materials acquire a higher yield stress.

The ultimate stacking height of R0 – R30 is 138, 140, 120, 117 mm, respectively. And the width of the bottom layer of each case is 30, 31, 33 and 33 mm, respectively. From these two respects, R20 and R30 produce both larger vertical and horizontal deformation than R0 and R10, which is mainly derived from the higher flowability and lower stiffness of R20 and R30. This analysis is also applicable to the final state of structures printed by R40 and R50, as shown in Fig. 6. The staked structures of R40 and R50 collapse with distorted shape due to the relatively high flowability and low stiffness. The final height of structures of R40 and R50 is 83 and 72 mm, respectively. Hence, mixtures of R40 and R50 are of low applicability to the developed 3D printer.

To quantitatively characterize the buildability, a factor ε_d is determined as the ratio of vertical deformation of the stacked twenty layers to the optimal height, i.e., 160 mm (8 mm × 20 layers). As results of the average strain and average thickness of each layer illustrated in Fig. 7(a), the shape retention of fresh mixtures decreases with the contents of tailings. Moreover, a parameter P_{hw} calculated by the height to width ratio is used to describe

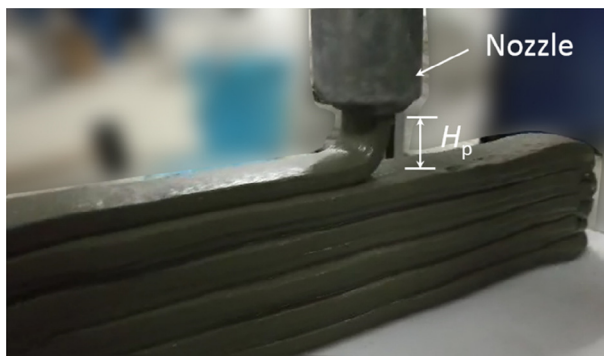


Fig. 5. The printing process. No-slump cement paste extruded from the nozzle can be considered as a relatively stiff continuous filament.

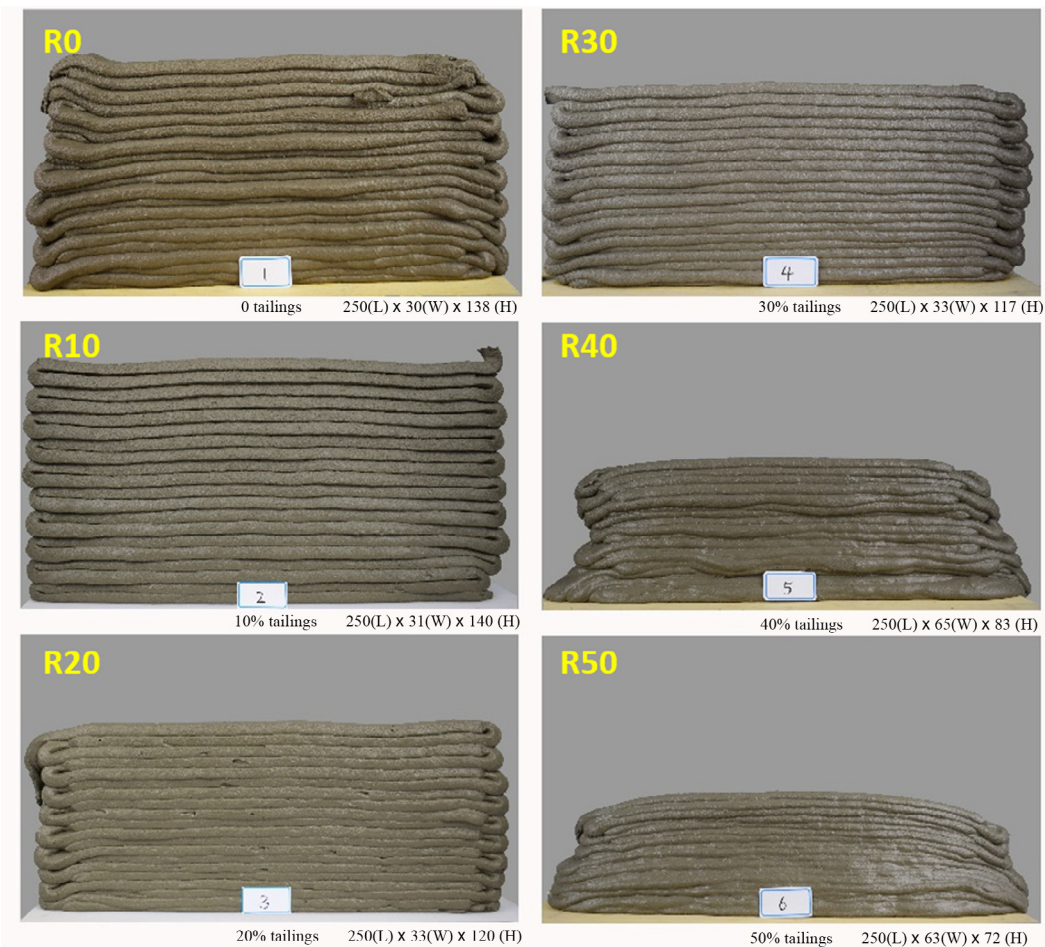


Fig. 6. Images of structures built-up with twenty layers of filament in a single process.

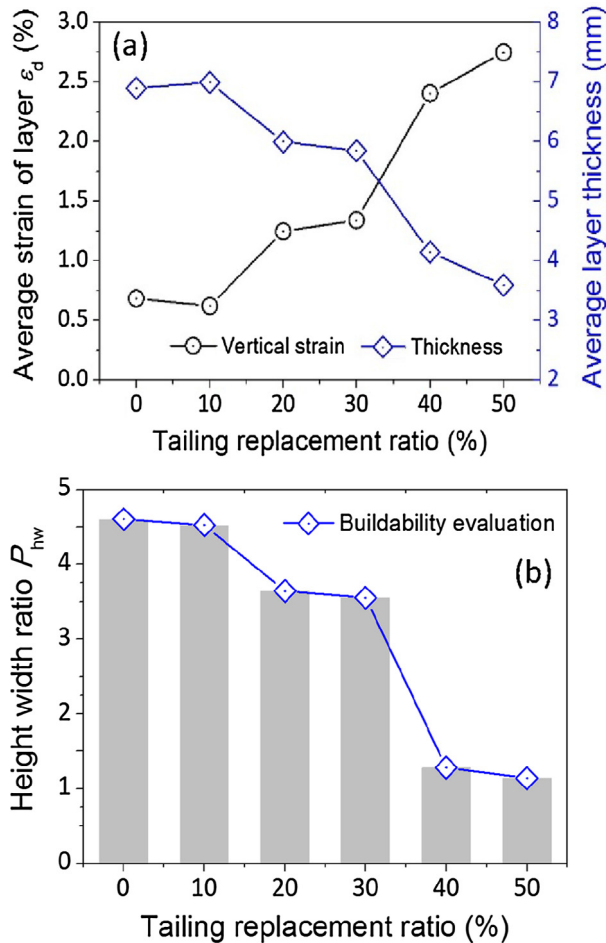


Fig. 7. (a) Vertical strain, average layer thickness and (b) height width ratio versus tailing replacement ratio.

the extent to which layers can be stacked. Fig. 7(b) depicts the results of P_{hw} , indicating that the structural or geometric stability of the printed structures decreases significantly with the dosage of tailings, especially from 30% to 40%. Additionally, it is noteworthy that some imperfections that induced by printer head inaccuracy, filament inconsistencies, or the dynamic deposition of filament may lead to premature collapse of the structure through instability during printing [41].

Based on the above analysis, a favorable stacking or the buildability is predominantly governed by the effective stiffness of the printed layers, which is on the premise of continuous extrusion of materials. Fig. 8 shows a 40 layers structure with height of 230 mm. It is clearly that the layers beneath those being printed are compressed due to their stiffness is not high enough to sustain the weight of subsequent layers. Each of these layers has a different stiffness $E(t)$ and flowability $F(t)$, both functions of their age t . Therefore, the rest time also plays a determinative effect on the buildability.

4.4. Open time evaluation

The open time is identified as the time interval during which the fresh concrete maintains good printability. Once disruption occurs in the extrusion process of filaments, open time is assumed ended. Fig. 9 illustrates the extruded filaments at different rest times, taking mixture R40 as an example. It can be seen that all the mixtures can be continuously printed out from the nozzle

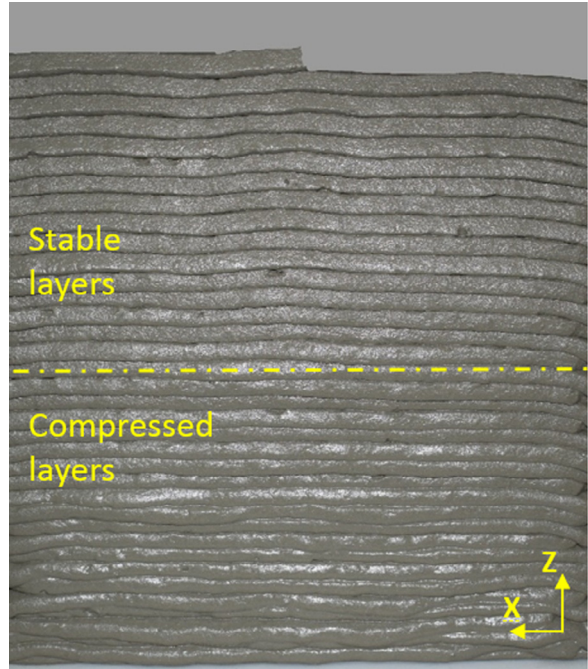


Fig. 8. Printed structure with dimension of 250(L) \times 33(W) \times 230(H) mm³.

within 80 min. However, the filament produce obvious disruption at rest time of 90 min, indicating the end of extrudability. In a similar way, the open time of R0–R30 and R50 is determined to be 90, 90, 90, 80, 70 min, respectively. Hence, a critical value of effective time for printing is recommended as 70 min. This indicates that cementitious materials with a rest time of less than 70 min can perform an acceptable extrudability.

From Fig. 9, the shape of the filament changes with the time. A parameter W is used to characterize the width of middle filament, and its changing trend with time is depicted in Fig. 10. The filament width significantly decreases when rest time is less than 30 min, and slightly decreases to the optimal width when the time is less than 80 min. The optimal width of filament equals to the width of the nozzle opening. This results reveal that within the time range of $t \leq 30$ min, the mixture performs favorable flowability. The mix shows satisfying shape retention (buildability) within the time range of $30 \text{ min} \leq t \leq 80$ min. The width-time curve serves as a powerful supplementary information for the buildability evaluation.

4.5. Flowability evaluation

Fig. 11 illustrates the slump test and jumping table test results of cementitious mixtures, respectively, varying with tailings replacement ratios and rest time from 10 to 90 mins. The rest time stands for the standing time immediately after the fresh mixture is manufactured. A larger slump value or spreading out diameter corresponds to a greater flowability and vice versa. It is shown that compared with the mixture with no tailing replacement, the flowability at a specific rest time increases with the replacing content of tailings to natural sand. At the rest time of 10 min, the drop in height of R0 – R50 are 5.8, 7.2, 7.7, 8.8, 9.5 and 9.8 mm, respectively. Substituting sand with 50% tailings improves the fluidity by 69.0% compared to the reference mix R0. At the same rest time, the spreading diameters of R0 – R50 are 19.2, 19.3, 20.5, 20.6, 21.8 and 22.1 mm, respectively. The spreading diameter of R50 is increased by 15.1% compared to R0. The results conform to the

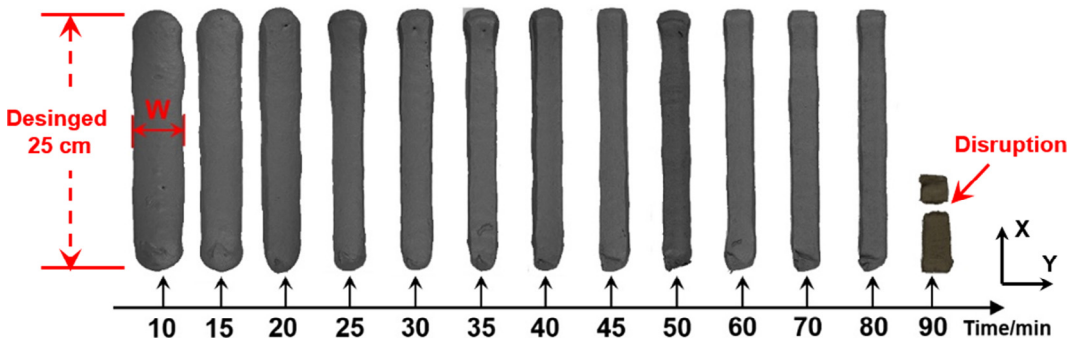


Fig. 9. Extruded filaments of mixture R40 at different rest times.

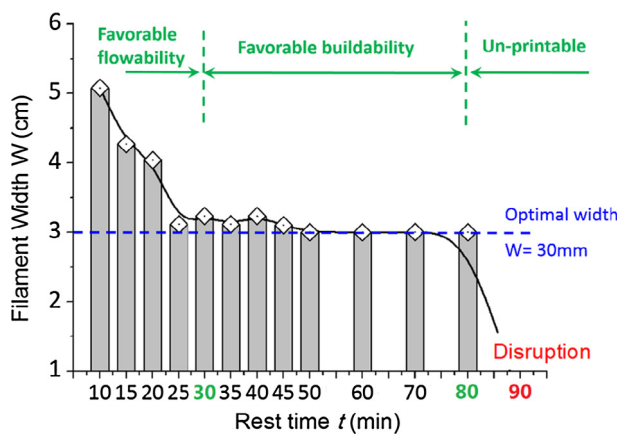


Fig. 10. Filament width of mix R40 changes with the rest time.

slump test analysis. However, it is found that the fluidity decreases with the increasing rest time. The spreading diameter of R0 – R50 is reduced by an average of 14.3% when prolonging the rest time from 10 min to 90 min. This is because a longer rest time of the cement-based materials promote the hydration degree of binding materials, and therefore the stiffness is gradually developed.

The slump test results provide supplementary references for the optimization of the extrudability and buildability of the materials for 3D printing. Increasing the tailing replacement ratio and shorten the rest time will facilitate a continuous and smooth extrusion process. In contrast, reducing the tailing percentage and prolonging the rest time can improve the stiffness and shape retention of the cementitious materials, therefore contributing to the buildability.

In addition, the cementitious material for 3D printing shall perform well with no significant segregation and jamming when passing through the narrow opening. The relationship of V funnel flow time varies with different tailing replacement ratios is presented in Fig. 12. The results show that replacing natural sands with tailings leads to the increasing elapsed time to flow through the V funnel, indicating a viscosity improvement. From the results, it takes the mixture of R0 and R50 22.1 and 26.4 s, respectively, to completely flow through the narrow opening of the V funnel. It indicates that the flow time is approximately prolonged by 20% when substitute sand with tailings from 0% to 50%. The analysis of particle size distribution, as shown in Fig. 4, shows the more tailings are used, the higher content of smaller size of particles will be, resulting in a requirement of higher water content and a larger inter-particle frictions. To a certain extent, replacing natural sand with tailing can increase the binding effect of cementitious materials between the adjacent printed layers, which is of great significance to

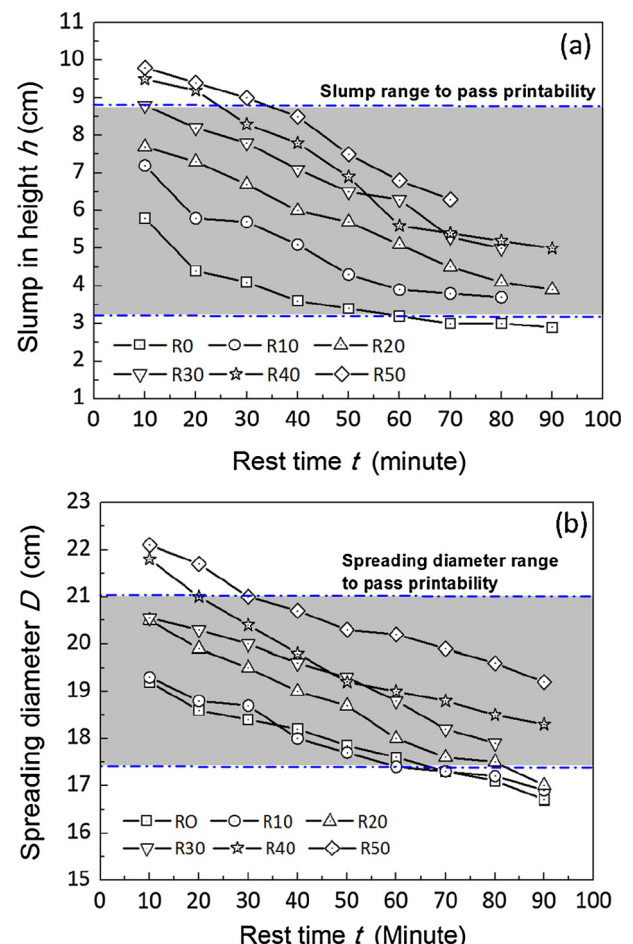


Fig. 11. (a) Slump and (b) spread out diameters of cementitious materials with different tailings replacement ratios varied with different rest times.

enhance the mechanical entirety and deformation resistance of the printed structures.

4.6. Structural build-up behavior evaluation

Penetration resistance method is preferable in accessing the stiffness development of cementitious materials at super-early ages due to its repeatability and easiness to implement. Fig. 13 presents the change of penetration resistance with the tailing content with rest time ranging from 10 min to 90 min. It can be seen that the penetration resistance grow approximately linearly with the rest time. The penetration resistance is a key parameter that quan-

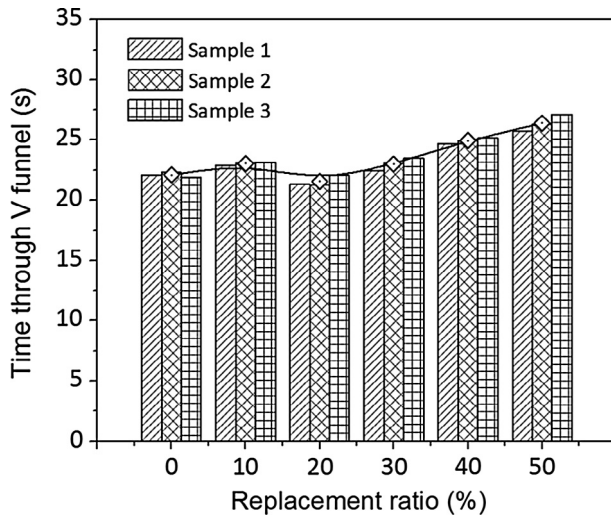


Fig. 12. Relationship of V funnel flow time varies with different tailing replacement ratios.

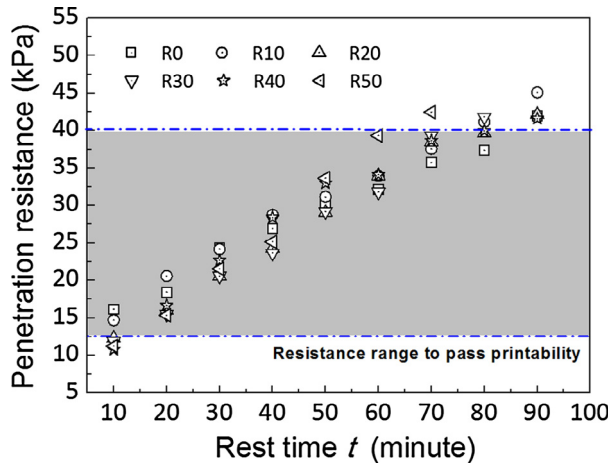


Fig. 13. Penetration resistance varying with tailing percentage and rest time in the preset state.

tifies the stiffness and strength development of cementitious materials and again it is directly related to the buildability of the printing materials. Based on the open time results, the extruded filament of mixtures with 0–50% replacement ratio of tailings to natural sand incurs disruption at the rest time of 90, 90, 90, 80, 90 and 70 min, respectively. At these times, corresponding penetration resistance of R0 – R50 are tested to be 41.9, 45.1, 42.1, 41.8, 41.6 and 42.5 kPa, respectively. Therefore, a critical value of penetration resistance C_p is determined as 40 kPa. Mixtures could not be printed continuously when their penetration resistances exceeds C_p . This demonstrates that cementitious materials with penetration resistance of less than 40 kPa can perform favorable extrudability.

The change of penetration resistance of various cementitious mixtures at rest times of several hours are also derived as shown in Fig. 14. The penetration resistance or the deformation resistance increase rapidly with the increasing rest time. The deformation resistance accounts for the resistant ability of the fresh material to the deformation induced by the applied loads[56]. 2 and 8 h after the manufacturing process completed, the penetration resistance of materials approximately reaches 50 kPa and 0.7 MPa, respectively. The average density of the cement mix is about 2.2

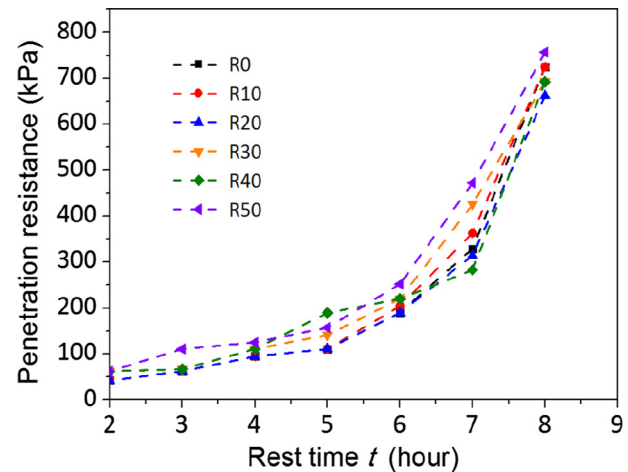


Fig. 14. Penetration resistance varied with tailing percentage at the rest time ranges from 2 to 8 h.

g/cm^3 and the volume of each layer is 75 cm^3 . Therefore, each printed layers can sustain more than one thousand subsequent layers at the rest time of 2 h. As cement hydrates, the cement paste evolves from a fluid to a plastic mass and finally to a rigid solid, and the bearing capacity rapidly increases with time. It is noteworthy that substituting tailing to sand does not significantly affect the setting behavior of the prepared materials. That is due to the cement content and water/binder ratio that directly related to the hydration process are fixed for all the mixtures in spite of that the sand/tailing ratio varies. The above analysis of cementitious materials is at their preset state, the hardened properties are discussed in the next section.

4.7. Mechanical property

Fig. 15 shows the compressive strength of specimens with different tailing contents at ages of 3, 14 and 28 days. The average strength of all the specimens is 36 MPa at 3 days after production. The high early age strength probably attributes to the content of 42.5 grade rapid setting cement. PP fibers also enhances and reinforces the mechanical properties by refraining deformation and crack propagation.

These results indicate that replacing natural sand with fine tailings does not have significant influence on the mechanical performance of materials at the age of 3 days. On the other hand, from the 14-day and 28-day results, the inclusion of fine tailings has a positive influence on the mechanical properties of the hardened materials when the replacement ratio is no more than 40%. The compressive strength of the hardened materials with tailing content of 40% at the age of 14 and 28 days are measured to be 47.0 and 53.2 MPa, respectively. And the strength of R40 is 21% and 23.2% higher than the counterparts with no tailing replacement. The tailing sand had an angular shaped surface[57]. The bite force between tailings particles can induce a better adhesion between paste and inclusions and lead to higher mechanical resistance to the applied load. The appropriate proportions of cement, silica fume and fly ash in combination with fine sands enable a high packing density of solid constituents, which contributes to strength development of tested materials.

Fig. 16(a) shows the prism specimens with corrugate surface cut from a 3D printed structure of mixture R30. The printed specimens are smoothed to eliminate the influence of corrugate surface on the fracture behaviors, as shown in Fig. 16(b), since that cracks are prone to initiate from the transition zones between two layers.

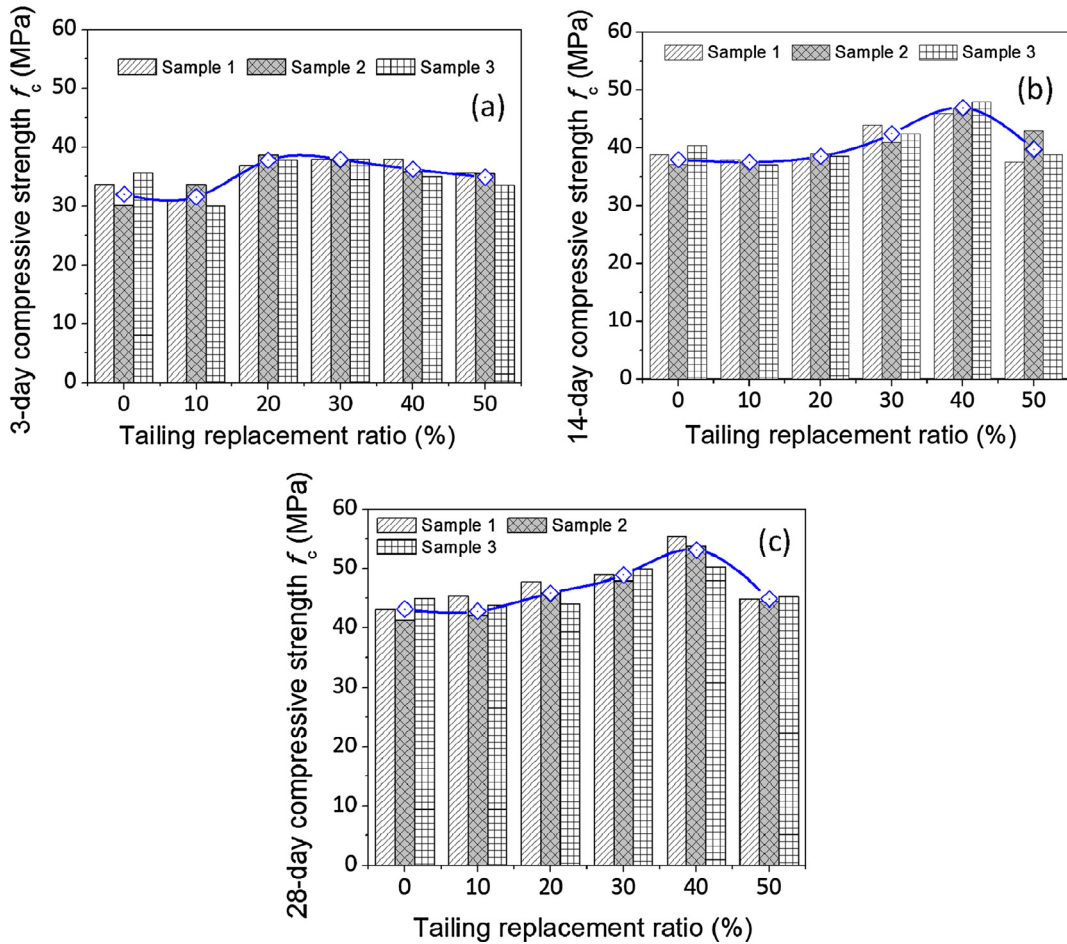


Fig. 15. Compressive strength of specimens with different tailing contents at the age of (a) 3 days, (b) 14 days, (c) 15 days.

The measured results of 7-day flexural strength and mid-span deflection between casted and printed specimens are depicted in Fig. 17. The average flexural strength and maximum deflection of printed samples are 31.4% and 36.3% lower than the casted samples, respectively. This demonstrates that the bending resistance of printed samples are weaker than the casted ones. It is mainly derived from the weaken interfaces, adhesion reduction or cold joints problems induced by the time gap between two successive filaments, which leads to a certain of mechanical losses [43,58]. Therefore, it is recommended to short the time of material to rest in the additive manufacturing process in order to reach a favorable structural integrality and loading capacity of printed structures. The 3D printing process of construction differs from the traditionally fabrication process. The bond strength between stacking layers relies on the specific treatment methods, such as viscosity modify agent (VMA) or proper curing method, to enhance the overall mechanical property by improving the structural integrity and mechanical properties of 3D printed structures.

4.8. Optimal design for 3D printed product

The optimal design of the printed products relies on the material fresh property and the printing process controlling (Fig. 18). The material parameters of slump, spreading diameter, open time, penetration resistance, viscous property and particle size distribution are highly dependent on the process parameters of printing speed V_p , extrusion rate V_e , nozzle opening O_z , print path P_L and print height H_p . Decreasing the slump character facilitates the mix to retain the printed geometry, thus contributing to the build-

ability. However, it may reduce the extrudability and even results in blockages. Prolonging the open time helps the mix keeping the surface chemically active to form strong interfaces between layers. On the other hand, it may sacrifice the stiffness development at early ages.

Therefore, in order to comprehensively access the printability of fresh mix, two coefficients P_E and P_B are introduced in this study to comprehensively access the printability of fresh mix. The extrudability is significantly governed by the flowability and the early-age stiffness. From our test results, the larger the flowability and the smaller the stiffness, the better the extrudability. Therefore, the extrudability is positive related to the ratio of flowability and stiffness. Due to the flowability can be characterized by the spreading diameter (D_s) and the structural build-up of the material (stiffness) is directly related to the time (t), the extrudability coefficient P_E is specified by the ratio of spreading diameter D_s and rest time t , as specified in Eq. (1). In terms of the buildability, it refers to the ability of material to retain its extruded shape and the resistance to the self-weight of subsequently deposited layers. A low slump of material indicates a favorable shape retention property. A high penetration resistance of material indicates a favorable resistance to the increased loads. Therefore, the buildability is positive related to the ratio of penetration resistance and slump. From our test results, the larger the penetration resistance and the smaller the slump, the better the buildability. Thus, the buildability coefficient P_B is specified by the ratio of the penetration resistance (P_r) and the slump (H_s) in our study, as expressed in Eq. (2).

A typical 3D printing process proceeds with that the material is continuously deposited by the movement of nozzle (extrud-

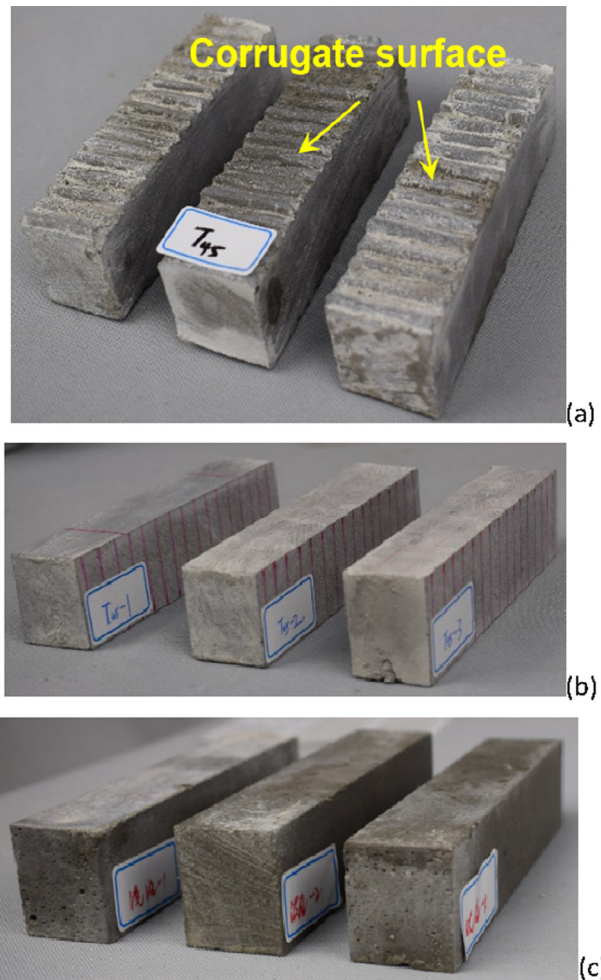


Fig. 16. (a) Prism specimens with corrugate surface cut from a 3D printed structure, (b) Surfaces of printed specimen were smoothed, (c) casted prism specimens.

ability) and stably built-up by stacking layers of the filaments (buildability). In general, optimizing design of printability primarily rely on the balance between the extrudability and buildability (Eq. (3)).

$$\text{Extrudability}(P_E) = \frac{\text{Flowability}(D_s)/\text{Time}(t)}{\text{Max}(D_s)/\text{Min}(t)} \times 100\% \quad (1)$$

$$\text{Buildability}(P_B) = \frac{\text{Stiffness}(P_r)/\text{Slump}(H_s)}{\text{Max}(P_r)/\text{Min}(H_s)} \times 100\% \quad (2)$$

$$\text{Printability}(P_P) = F_{\text{optimal}}(P_E, P_B) \quad (3)$$

The definition of the buildability and extrudability coefficients are from an experimental point of view. From our investigations, they are applicable and effective to evaluate the printability of fresh cement mortars. Fig. 19(a) depicts the time-history of material parameter D_s , H_s , P_r of mix R40. Based on these data, the buildability coefficients P_B and extrudability coefficients P_E can be obtained by substituting parameters of D_s , H_s , P_r and t into Eqs. (1) and (2) (see Fig. 19(b)). The extrudability decreases with the rest time, while the buildability performs an opposite trend. The results also indicate that the better the extrudability, the worse the buildability, and vice versa. A optimal point is specified as the crossing points of P_E and P_B curves, which indicates that the rest time of mixture R40 shall be controlled at 30 min. The optimal

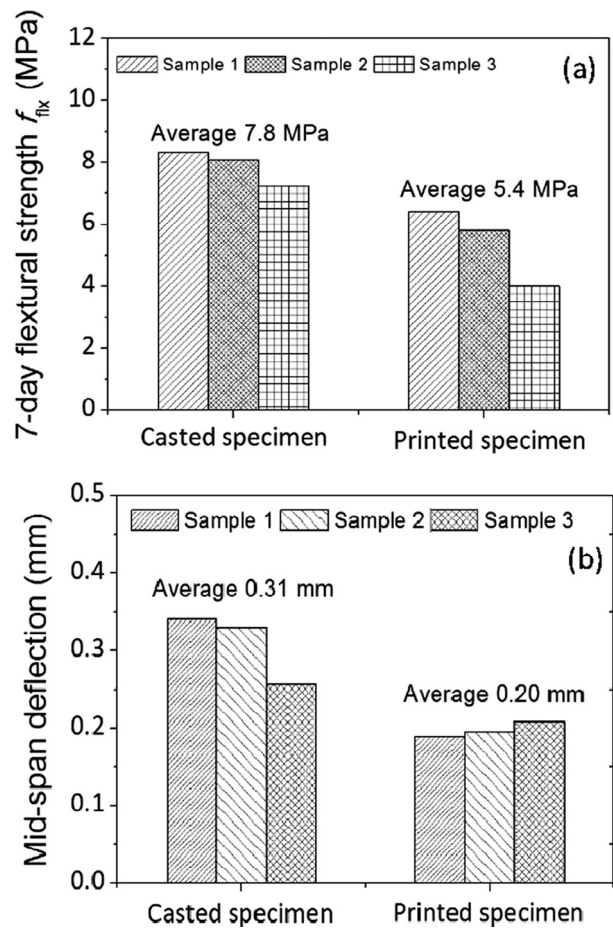


Fig. 17. Comparison of (a) 7-day flexural strength and (b) mid-span deflection between casted and printed specimens.

rest time of R50 is obtained in a similar manner, which is identified as 40 min. Therefore, structures of R40 and R50 are re-printed by extending the rest time from previous 10 min to 30 min and 40 min, respectively, as illustrated in Fig. 20. Similarly, 20 layers are stacked. The printing speed is also controlled as 450 cm/min in the horizontal direction and 1.3 cm/min in the vertical direction. It can be seen that the modified mixtures show good buildability. After change the rest time, the stacking height of R40 increases from 83 mm to 139 mm, and stacking height of R50 increases from 72 mm to 118 mm, both prove the effectiveness of the proposed optimizing method.

5. Conclusions

Six trial mixes with different substituting mass ratio of copper tailing to natural sand are used to identify the optimum mix proportions for extrusion based printing. The following conclusions have been derived from the current research:

- (1) A simply equipped printing system is designed in the present study to investigate the printable behaviors of fresh paste and the processing parameters of the 3D printer. The extrusion rate V_e is determined as 5.4 Liters/minute, the printing speed V_p is controlled as 75 mm/s in the horizontal direction and 13 mm/min in the vertical direction, and the printing height H_p is set as 24 mm to facilitate the printing process.

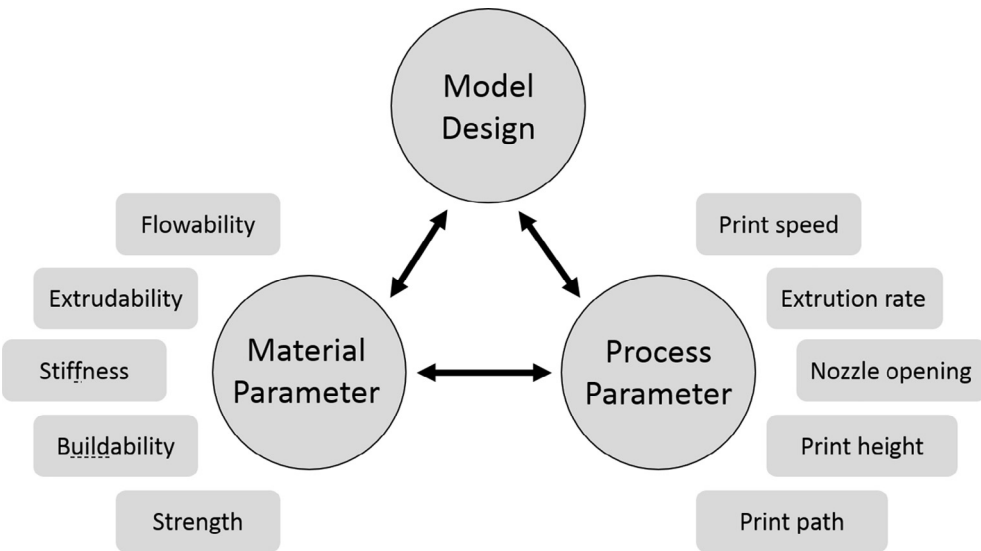


Fig. 18. Chart of Interdependent parameters for product design material property and process controlling.

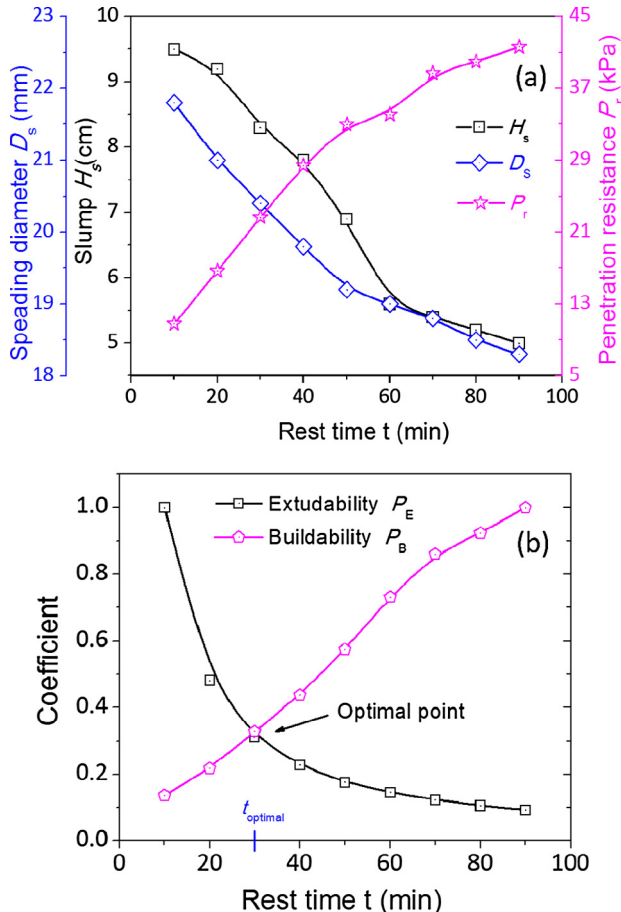


Fig. 19. (a) Material parameter D_s , H_s , P_r of mix R40 versus time t ; (b) breakeven relationship of extrudability and buildability of mix R40.

- (2) Due to the finer particle of copper tailings, the flowability of fresh paste characterized by the slump, spreading diameter and V funnel time increases with the replacement ratio of tailings. The buildability characterized by the penetration resistance and height/ width ratio P_{hw} decreases with the replacement ratio of tailings.

(3) The open time of all the mixtures is determined as 70 min, after which the filament cannot be continuously deposited. The mixtures of R40 and R50 are of low applicability for build-up structures due to their relatively high flowability and low stiffness at early ages. Based on above two aspects, the range of slump H_s , spreading diameter D_s and penetration resistance P_r of wet mix to pass printability are recommended as 32–88 mm, 174–210 mm and 13–40 kPa, respectively. The fresh properties of optimal mix shall meet these requirements.

(4) To conclude the present research, an optimizing design method is first proposed by evaluating the parameters of extrudability coefficients P_E and buildability coefficients P_B , both of which comprehensively take the relevant material fresh properties of flowability, stiffness and setting behaviors into account. The low buildable mixtures R40 and R50 can be re-printed to satisfy structures by adjusting the rest time to the calculated optimal value by the proposed method.

(5) Tests show that the mix R30 is the best choice of printing freeform components, which has a water-binder ratio of 0.26 and sand-tailing ratio of 3:2, comprising 70% cement, 20% fly ash and 10% silica fume, plus 1.2 kg/m³ micro polypropylene fibers. This mix also needed 1.083% superplasticizer and to attain an optimum workability.

(6) The average flexural strength and maximum deflection of the printed samples are 31.4% and 36.3% lower than the casted counterparts, respectively, demonstrating a lower bending resistance of printed samples than the casted ones.

Future research will be devoted to experimental study to find the relation between mixture design, printing behavior and mechanical properties of materials for printing. Particularly, it should pay much attention to elucidate the influence of yield stress evolution of cementitious materials and the time gap between two adjacent layers on the structural stability and integrality of printed structures in order to provide better basis for printability controlling. Since the current printed objects are either unreinforced, or reinforcement is applied manually, fiber reinforced mixtures that increases the ductility of the printed concrete will be developed. Further research will also be carried out to explore the frontiers

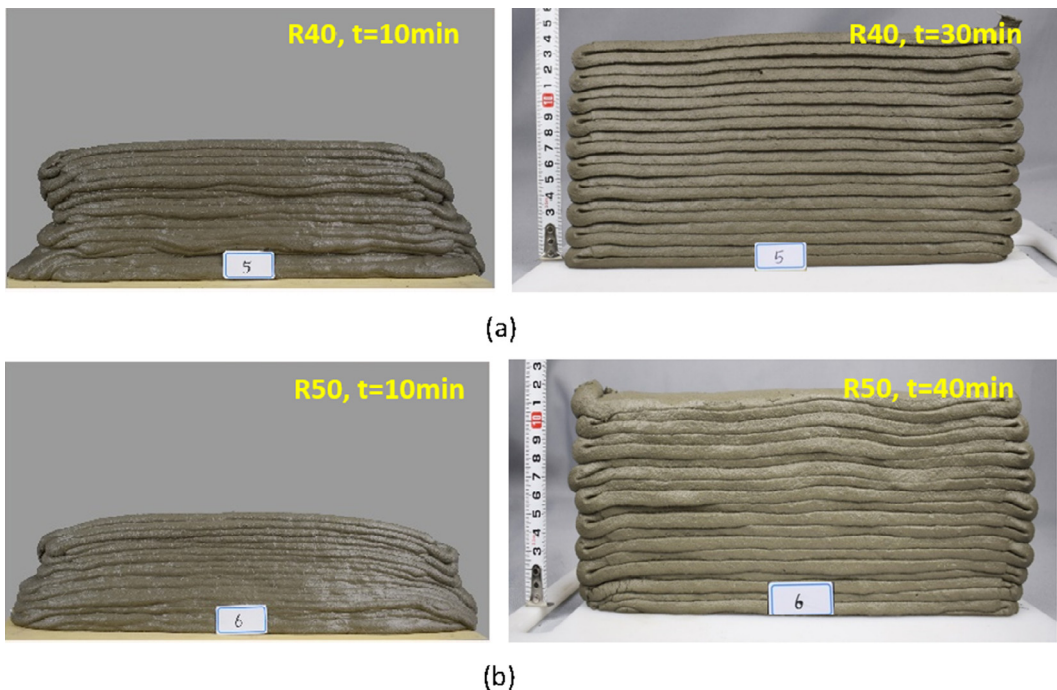


Fig. 20. Structure of mixture (a) R40 and (b) R50 are re-printed after rest time is extended to the optimal time.

of 3D printing and promote its effective application in the real life construction sectors.

Acknowledgment

The authors would like to acknowledge the support by the National Major Research Instrument Development Project of the National Natural Science Foundation of China (Grant No. 51627812), and the opening project of State Key Laboratory of Explosion Science and Technology (Beijing Institute of Technology, Grant No. KFJJ13-11M).

References

- [1] F. Rengier, A. Mehndiratta, H.V. Tengkobligk, C.M. Zechmann, R. Unterhinninghofen, H.U. Kauczor, F.L. Giesel, 3D printing based on imaging data: review of medical applications, *Int. J. Comput. Assist. Radiol. Surg.* 5 (4) (2010) 335–341.
- [2] B. Utela, D. Storti, R. Anderson, M. Ganter, A review of process development steps for new material systems in three dimensional printing (3DP), *J. Manuf. Process* 10 (2) (2008) 96–104.
- [3] X.L. Ma, Research on application of SLA technology in the 3D printing technology, *Appl. Mech. Mater.* 401–403 (2013) 938–941.
- [4] H.N. Chia, B.M. Wu, Recent advances in 3D printing of biomaterials, *J. Biol. Eng.* 9 (1) (2015) 1–14.
- [5] V.N. Nerella, M. Krause, M. Näther, V. Mechtcherine, Studying printability of fresh concrete for formwork free Concrete on-site 3D Printing technology (CONPrint3D), in: Conference on Rheology of Building Materials, 2016.
- [6] W. Gao, Y. Zhang, D. Ramanujan, K. Raman, Y. Chen, C.B. Williams, C.C.L. Wang, Y.C. Shin, S. Zhang, P.D. Zavattieri, The status, challenges, and future of additive manufacturing in engineering, *Comp. Aided Des.* 69 (2015) 65–89.
- [7] R.A. Buswell, R.C. Soar, A.G.F. Gibb, A. Thorpe, Freeform Construction: Mega-scale Rapid Manufacturing for construction, *Autom. Constr.* 16 (2) (2007) 224–231.
- [8] I. Perkins, M. Skitmore, Three-dimensional printing in the construction industry: a review, *Int. J. Constr. Manag.* 15 (1) (2015) 1–9.
- [9] B. Khoshnevis, Automated construction by contour crafting—related robotics and information technologies, *Autom. Constr.* 13 (1) (2004) 5–19.
- [10] Winsun, WinSun China builds world's first 3D printed villa and tallest 3D printed apartment building, <http://www.3ders.org/articles/20150118-winsun-builds-world-first-3d-printed-villa-and-tallest-3d-printed-building-in-china.html> (2015).
- [11] WASP, The first adobe building, <http://www.wasproject.it/w/en/3d-printers-projects/> (2016).
- [12] A. Rudenko, 3D concrete house printer, <http://www.designboom.com/technology/3d-printed-concrete-castle-minnesota-andrey-rudenko-08-28-2014/> (2015).
- [13] T.T. Le, S.A. Austin, S. Lim, R.A. Buswell, A.G.F. Gibb, T. Thorpe, Mix design and fresh properties for high-performance printing concrete, *Mater. Struct.* 45 (8) (2012) 1221–1232.
- [14] P. Shakor, J. Sanjayan, A. Nazari, S. Nejadi, Modified 3D printed powder to cement-based material and mechanical properties of cement scaffold used in 3D printing, *Constr. Build. Mater.* 138 (2017) 398–409.
- [15] M. Hambach, D. Volkmer, Properties of 3D-printed fiber-reinforced Portland cement paste, *Cem. Conc. Comp.* 79 (2017) 62–70.
- [16] C. Gosselin, R. Dubal, P. Roux, N. Gaudilliére, J. Dirrenberger, P. Morel, Large-scale 3D printing of ultra-high performance concrete—a new processing route for architects and builders, *Mater. Des.* 100 (2016) 102–109.
- [17] B.J. Burd, Evaluation of mine tailings effects on a benthic marine infaunal community over 29 years, *Mar. Environ. Res.* 53 (5) (2002) 481–519.
- [18] Y. Chen, Y. Zhang, T. Chen, Y. Zhao, S. Bao, Preparation of eco-friendly construction bricks from hematite tailings, *Constr. Build. Mater.* 25 (4) (2011) 2107–2111.
- [19] R.G. Gopez, Utilizing mine tailings as substitute construction material: the use of waste materials in roller compacted concrete, *Open Access Library J.* 2 (12) (2015) 1–9.
- [20] L. Zhang, S. Ahmari, J. Zhang, Synthesis and characterization of fly ash modified mine tailings-based geopolymers, *Constr. Build. Mater.* 25 (9) (2011) 3773–3781.
- [21] C.L. Wang, W. Ni, S.Q. Zhang, S. Wang, G.S. Gai, W.K. Wang, Preparation and properties of autoclaved aerated concrete using coal gangue and iron ore tailings, *Constr. Build. Mater.* 104 (2016) 109–115.
- [22] X.-Y. Huang, W. Ni, W.-H. Cui, Z.-J. Wang, L.-P. Zhu, Preparation of autoclaved aerated concrete using copper tailings and blast furnace slag, *Constr. Build. Mater.* 27 (1) (2012) 1–5.
- [23] S. Ahmari, L. Zhang, Production of eco-friendly bricks from copper mine tailings through geopolymerization, *Constr. Build. Mater.* 29 (2012) 323–331.
- [24] L. Cai, B. Ma, X. Li, Y. Lv, Z. Liu, S. Jian, Mechanical and hydration characteristics of autoclaved aerated concrete (AAC) containing iron-tailings: effect of content and fineness, *Constr. Build. Mater.* 128 (2016) 361–372.
- [25] S. Zhao, J. Fan, W. Sun, Utilization of iron ore tailings as fine aggregate in ultra-high performance concrete, *Constr. Build. Mater.* 50 (2) (2014) 540–548.
- [26] G.J. Gibbons, R. Williams, P. Purnell, E. Farahi, 3D Printing of cement composites, *Adv. Appl. Ceram.* 109 (5) (2010) 287–290.
- [27] S. Lim, R.A. Buswell, T.T. Le, S.A. Austin, A.G.F. Gibb, T. Thorpe, Developments in construction-scale additive manufacturing processes, *Autom. Constr.* 21 (2012) 262–268.
- [28] S. Lim, R.A. Buswell, P.J. Valentine, D. Piker, S.A. Austin, X. De Kestelier, Modelling curved-layered printing paths for fabricating large-scale construction components, *Addit. Manuf.* 12 (Part B) (2016) 216–230.
- [29] ASTM Standard C1611/C1611M-14, Standard Test Method for Slump Flow of Self-Consolidating Concrete, ASTM International, West Conshohocken, PA, 2003, www.astm.org.

- [30] G. Ma, L. Wang, Y. Ju, State-of-the-art of 3D printing technology of cementitious material – an emerging technique for construction, *Sci. China Tech. Sci.* (2017), <https://doi.org/10.1007/s11431-016-9077-7>.
- [31] A. Kazemian, X. Yuan, E. Cochran, B. Khoshnevis, Cementitious materials for construction-scale 3D printing: laboratory testing of fresh printing mixture, *Constr. Build. Mater.* 145 (2017) 639–647.
- [32] H. Zhao, W. Sun, X. Wu, B. Gao, The effect of coarse aggregate gradation on the properties of self-compacting concrete, *Mater. Des.* 40 (2012) 109–116.
- [33] W.B. Ashraf, M.A. Noor, Performance-evaluation of concrete properties for different combined aggregate gradation approaches, *Procedia Eng.* 14 (Suppl. C) (2011) 2627–2634.
- [34] P. Wu, J. Wang, X. Wang, A critical review of the use of 3-D printing in the construction industry, *Autom. Constr.* 68 (2016) 21–31.
- [35] Z. Malaeb, H. Hachem, A. Tourbah, T. Maalouf, N.E. Zarwi, F. Hamzeh, 3D concrete printing: machine and mix design, *Int. J. Civil Eng.* 6 (6) (2015) 14–22.
- [36] A. Perrot, D. Rangeard, Y. Melinge, Prediction of the ram extrusion force of cement-based materials, *Appl. Rheol.* 24 (5) (2015) 53320.
- [37] A. Perrot, C. Lanos, P. Estellé, Y. Melinge, Ram extrusion force for a frictional plastic material: model prediction and application to cement paste, *Rheol. Acta* 45 (4) (2006) 457–467.
- [38] A. Perrot, Y. Mélinge, P. Estellé, C. Lanos, Modeling the ram extrusion force of a frictional plastic material, 2006.
- [39] A. Perrot, Y. Mélinge, D. Rangeard, F. Micaelli, P. Estellé, C. Lanos, Use of ram extruder as a combined rheo-tribometer to study the behaviour of high yield stress fluids at low strain rate, *Rheol. Acta* 51 (8) (2012) 743–754.
- [40] A. Perrot, D. Rangeard, A. Pierre, Structural built-up of cement-based materials used for 3D-printing extrusion techniques, *Mater. Struct.* 49 (4) (2016) 1–8.
- [41] F. Bos, R. Wolfs, Z. Ahmed, T. Salet, Additive manufacturing of concrete in construction: potentials and challenges of 3D concrete printing, *Virt. Phys. Prototyp.* 11 (3) (2016) 209–225.
- [42] A.M. Alhozaimy, Effect of absorption of limestone aggregates on strength and slump loss of concrete, *Cem. Conc. Comp.* 31 (7) (2009) 470–473.
- [43] T. Wangler, E. Lloret, L. Reiter, F. Gramazio, M. Kohler, M. Bernhard, B. Dillenburger, J. Buchli, N. Roussel, Digital concrete: opportunities and challenges, *RILEM Tech. Lett.* 1 (2016) 67–75.
- [44] N. Roussel, F. Cussigh, Distinct-layer casting of SCC: The mechanical consequences of thixotropy, *Cem. Conc. Res.* 38 (5) (2008) 624–632.
- [45] Chinese National Standard, Ready-mixed concrete, GB/T 14902-2012.
- [46] Chinese industry standards, JGJ/T283-2012, Technical specification for application of self-compacting concrete, 2012.
- [47] Chinese National Testing Standard, GB/T 2419-2005, Test method for fluidity of cement mortar.
- [48] M. Lachemi, K.M.A. Hossain, V. Lambros, P.C. Nkinamubanzi, N. Bouzoubaâ, Self-consolidating concrete incorporating new viscosity modifying admixtures, *Cem. Conc. Res.* 34 (6) (2004) 917–926.
- [49] Chinese National Testing Standard, Standard for test method of performance on ordinary fresh concrete, GB/T 50080-2002.
- [50] X.L. Zhao, Y. Bai, L.C. Zhou, J. Shi, H.W. Kuang, Applicability research for masonry mortar compressive strength curve using penetration resistance method, 2nd International Conference on Mechanical Engineering, Industrial Electronics and Informatization, MEIEI 2013, September 14, 2013 – September 15, 2013, Trans Tech Publications Ltd, Chongqing, China, 2013, pp. 325–328.
- [51] Y. Liao, X. Wei, Penetration resistance and electrical resistivity of cement paste with superplasticizer, *Mater. Struct.* 47 (4) (2014) 563–570.
- [52] Chinese national testing standard, Standard for test method of mechanical properties on ordinary concrete, GB/T 50081-2002.
- [53] Totalkustom.com, <http://www.totalkustom.com/3d-castle-completed.html>, 2016.
- [54] R. Wolfs, T.T. Salet, An optimization strategy for 3D concrete printing, *Proceedings of the 22nd EG-ICE workshop 2015*, Eindhoven (2015).
- [55] D. Hwang, B. Khoshnevis, D.J. Epstein, Concrete wall fabrication by contour crafting., 21st International Symposium on Automation and Robotics in Construction (ISARC 2004), Jeju (2004).
- [56] Y.S. Doh, K.K. Yun, S.N. Amirkhanian, K.W. Kim, Framework for developing a static strength test for measuring deformation resistance of asphalt concrete mixtures, *Constr. Build. Mater.* 21 (12) (2007) 2047–2058.
- [57] A.U. Shettima, M.W. Hussin, Y. Ahmad, J. Mirza, Evaluation of iron ore tailings as replacement for fine aggregate in concrete, *Constr. Build. Mater.* 120 (Suppl. C) (2016) 72–79.
- [58] T.T. Le, S.A. Austin, S. Lim, R.A. Buswell, R. Law, A.G.F. Gibb, T. Thorpe, Hardened properties of high-performance printing concrete, *Cem. Conc. Res.* 42 (3) (2012) 558–566.